

# Sparse Interaction Neighborhood Selection for Markov Random Fields via Reversible Jump and Pseudoposteriors

Victor Freguglia      Nancy Lopes Garcia  
University of Campinas      University of Campinas

May 1, 2024

## Abstract

We consider the problem of estimating the interacting neighborhood of a Markov Random Field model with finite support and homogeneous pairwise interactions based on relative positions of a two-dimensional lattice. Using a Bayesian framework, we propose a Reversible Jump Monte Carlo Markov Chain algorithm that jumps across subsets of a maximal range neighborhood, allowing us to perform model selection based on a marginal pseudoposterior distribution of models. To show the strength of our proposed methodology we perform a simulation study and apply it to a real dataset from a discrete texture image analysis.

## 1 Introduction

Markov Random Fields (MRFs) on two-dimensional lattices are popular probabilistic models for describing features of digital images in a wide range of applications. Classical problems like image segmentation rely on these models to describe unobserved variables used for pixel classification, see for example [Held et al. \(1997\)](#); [Zhang et al. \(2001\)](#). More general inference-oriented models, such as the ones used in texture modeling problems, describe pixel values directly as a Markov Random Field with pioneer works by [Hassner and Sklansky \(1981\)](#); [Cross and Jain \(1983\)](#). We recommend the comprehensive reviews by [Blake et al. \(2011\)](#) and [Kato et al. \(2012\)](#), particularly in image processing and segmentation.

The wide applicability of MRFs is not the only reason that generates interest in the study of such models, rather, it is coupled with many theoretical and computational challenges posed when handling high dimensional data. More specifically, a Markov Random Field in a lattice is a collection of random variables whose dependence structure is implicitly defined by a graph. Even when the edge structure is completely known, one of the main inferential challenges is caused by cycles that prevent expressing the likelihood function as a product

of simpler conditional probabilities as in classical Markov Chain models. The impossibility of decomposing the joint probability of a high-dimensional random vector into simpler pieces requires a high-dimensional integral (or sum) in order to compute the normalizing constant of those probability measures. In general, the normalizing constant directly depends on the parameters of the distribution, thus being an important part of likelihood-based analyses. Whenever this high-dimensional integral cannot be computed in reasonable time, often due to the exponential complexity of a non-independent high-dimensional space, the likelihood function becomes intractable, rendering most of the usual inference and model selection techniques unusable directly.

Inference under intractable likelihoods is a key topic for analyzing high-dimensional data with local dependence. Several authors have proposed to approximate ratios of the normalizing constants (Geyer and Thompson, 1992; Gelman and Meng, 1998) or other approximating methods such as stochastic approximation (Gu and Zhu, 2001), thermodynamic integration (Green and Richardson, 2002) or continuous Contour Monte Carlo (Liang, 2007). However, most methods use Monte Carlo simulations which become extremely expensive for very large lattices. More recently, Zhu and Fan (2018) proposed a new approach that can be feasible by decomposing a large lattice into smaller sublattices. Under the Bayesian paradigm, Monte Carlo Markov Chain (MCMC) methods that generate samples from the posterior distributions under intractability have been developed using different strategies, such as including additional random elements with particular distributions that lead to convenient analytical properties that cancels out the intractable constant (Murray et al., 2012) or generating samples from model configurations that help producing approximations for the intractable likelihood function at each step of the MCMC algorithm (Atchadé et al., 2013) or prior to the Markov Chain iterations (Boland et al., 2018).

Another frequently used approach, introduced in Besag (1975), is to directly substitute the likelihood function term that appears in the posterior distribution for the pseudolikelihood function resulting in an analysis based not on the posterior distribution, but on a function that is referred as the pseudoposterior distribution. While the pseudolikelihood function may differ from the actual likelihood function, inference methods based on pseudolikelihoods have theoretical results available and practical usefulness, including in Bayesian contexts, often including adjustments to the function such as in Bouranis et al. (2017).

Furthermore, the selection of the neighborhood system adds a critical challenge, when dealing with the intractability of likelihood in Markov Random Fields, impeding the use of the common methodologies for model selection. Although using an approximation of the likelihood function removes most of the probabilistic properties which model selection and hypothesis testing in general rely on, in the context of determining the neighborhood for MRF, pseudolikelihoods have been used by several authors. Among others, we can cite the early work of Ji and Seymour (1996) which proposed its use for Gibbs random fields induced by translation-invariant pair-potentials of finite range, to more recent works, such as Lee and Hastie (2013) which designed algorithms for structure

learning in graphical models and, [Su and Borsuk \(2016\)](#), [Pensar et al. \(2017\)](#) and [Roy and Dunson \(2020\)](#) that used pseudoposteriors to find the dependence structure in Markov networks (graphical models). It is worth noticing that [Csiszár and Talata \(2006\)](#) proved that a modification of the Bayesian Information Criteria, replacing the likelihood by the pseudolikelihood, provides strongly consistent estimators of the neighborhood from a single realization of the process observed at increasing regions.

Studying complex models under a Bayesian framework offers distinct advantages, particularly in extending the space of unobserved random quantities to include not only a vector of real-valued parameters, but also more general objects that can represent models. By incorporating subsets of an arbitrary parameter space and using MCMC methods to obtain the distribution from these general objects, it becomes more feasible than constructing efficient optimizations algorithm within such spaces. For example, [Arnesen and Tjelmeland \(2017\)](#) aims to select the dependence structure of an Ising model among a small set of possible candidates with low-dimensional parameter spaces. Additionally, RJMCMC methods ([Green, 1995](#)) provide a framework for constructing a Markov Chain with a generic invariant distribution on general spaces, including varying-dimensional parameter spaces which are useful for variable and model selection under a Bayesian paradigm. However, the efficiency of these methods relies heavily on the careful construction of a proposal kernel. For instance, [Bouranis et al. \(2018b\)](#) proposes a RJMCMC model selection procedure for the exponential random graph model.

Our contribution on this topic is to propose a pseudoposterior-based procedure for selecting the interaction structure from a large set of candidate subsets of a maximal structure within a general class of Markov Random Field models with pairwise interactions. This selection is based on a set of relative positions, as introduced in [Section 2](#), using RJMCMC with a kernel specially constructed for this purpose, as detailed in [Section 3](#). To show the strength of our method, we conducted a simulation study, presented in [Section 4](#), under different scenarios and apply the algorithm to a texture synthesis problem with a real-world data in [Section 5](#).

## 2 Markov Random Fields with Spatially Homogeneous Pairwise Interactions

### 2.1 Model Description and Definitions

Consider a Markov Random Field (MRF) model on two-dimensional lattices with finite support and non-parametric pairwise interactions as described in [Freguglia et al. \(2020\)](#). The probability function for this model is completely defined by two main elements: *a set of relative positions*, that described the interaction structure of the process, and *a vector of potentials* describing the weights of interactions for each of these relative positions.

Denote by  $\mathcal{S}$  a set of sites (also referred as pixels) in a finite  $n_1$  by  $n_2$  two-dimensional lattice

$$\mathcal{S} = \{\mathbf{i} = (i_1, i_2) : 1 \leq i_1 \leq n_1, 1 \leq i_2 \leq n_2\},$$

and  $\mathbf{Z} = (Z_{\mathbf{i}})_{\mathbf{i} \in \mathcal{S}}$  a random field indexed by  $\mathcal{S}$ , where each  $Z_{\mathbf{i}}$  is a random variable assuming values in a finite alphabet denoted  $\mathcal{Z}$ . Without loss of generality, we consider  $\mathcal{Z} = \{0, 1, \dots, C\}$ .

Define a *Relative Position Set (RPS)*, denoted  $\mathcal{R}$ , as a finite set of integer vectors  $\mathbf{r} \in \mathbb{Z}^2$  without pairs of vectors with opposing directions, i.e.,

$$\mathbf{r} \in \mathcal{R} \implies -\mathbf{r} \notin \mathcal{R},$$

and, given a fixed RPS  $\mathcal{R}$ , define a vector of potentials denoted  $\boldsymbol{\theta}$ , as a vector of real numbers indexed by  $\mathcal{Z} \times \mathcal{Z} \times \mathcal{R}$ ,

$$\boldsymbol{\theta} = (\theta_{a,b,\mathbf{r}})_{a,b \in \mathcal{Z}, \mathbf{r} \in \mathcal{R}}.$$

Given a RPS  $\mathcal{R}$  and an associated vector  $\boldsymbol{\theta}$ , the Markov Random Field with homogeneous pairwise interaction considered in this work is characterized by the probability measure

$$f(\mathbf{z}|\mathcal{R}, \boldsymbol{\theta}) = \frac{1}{\zeta(\boldsymbol{\theta})} \exp \left( \sum_{\mathbf{i} \in \mathcal{S}} \sum_{\mathbf{r} \in \mathcal{R}} \sum_{a=0}^C \sum_{b=0}^C \theta_{a,b,\mathbf{r}} \mathbb{1}_{(z_{\mathbf{i}}=a)} \mathbb{1}_{(z_{\mathbf{i}+\mathbf{r}}=b)} \right), \quad (1)$$

where  $\zeta(\boldsymbol{\theta}) = \sum_{\mathbf{z}' \in \mathcal{Z}^{|\mathcal{S}|}} \exp \left( \sum_{\mathbf{i} \in \mathcal{S}} \sum_{\mathbf{r} \in \mathcal{R}} \sum_{a=0}^C \sum_{b=0}^C \theta_{a,b,\mathbf{r}} \mathbb{1}_{(z'_{\mathbf{i}}=a)} \mathbb{1}_{(z'_{\mathbf{i}+\mathbf{r}}=b)} \right)$  is a normalizing constant, with the convention that the term  $\mathbb{1}_{(z'_{\mathbf{i}}=a)}$  is treated as 0 if  $\mathbf{i}' \notin \mathcal{S}$  for every  $a \in \mathcal{Z}$ . This ensures that the sum terms are consistently defined across every pair of positions in  $\mathcal{S}$  that are within a relative position in  $\mathcal{R}$ . **Figure 1** presents an illustration of how the terms  $\sum_{\mathbf{r} \in \mathcal{R}} \theta_{z_{\mathbf{i}}, z_{\mathbf{i}+\mathbf{r}}, \mathbf{r}}$  are computed for some positions  $\mathbf{i}$  of an example field  $\mathbf{z}$ .

In (1), adding a constant value to the potentials  $\theta_{a,b,\mathbf{r}}$  associated with every pair  $a, b \in \mathcal{Z}$  and a fixed relative position  $\mathbf{r}$ , causes the value of  $f(\mathbf{z}, \mathcal{R}, \boldsymbol{\theta})$  to be unchanged, as the resulting scale change is also reflected in the normalizing constant  $\zeta(\boldsymbol{\theta})$ . In other words, two different vector of potentials  $\boldsymbol{\theta}$  may have the same likelihood, therefore, leading to a non-identifiability problem. In order to obtain identifiability, additional constraints are required and, following [Freguglia et al. \(2020\)](#), we adopt the zero-valued reference pair  $((a, b) = (0, 0))$  constraint

$$\theta_{0,0,\mathbf{r}} = 0 \text{ for all } \mathbf{r} \in \mathcal{R}.$$

Note that, while we still use the term  $\theta_{0,0,\mathbf{r}}$  in some equations, for simplicity of notation, we will not consider these indexes in the vector  $\boldsymbol{\theta}$ . Additionally, the vector  $\boldsymbol{\theta}$  can be expressed in terms of subvectors  $\boldsymbol{\theta} = (\boldsymbol{\theta}_{\mathbf{r}})_{\mathbf{r} \in \mathcal{R}}$ , where each subvector  $\boldsymbol{\theta}_{\mathbf{r}} = (\theta_{a,b,\mathbf{r}})_{(a,b) \in \mathcal{Z}^2, (a,b) \neq (0,0)}$  corresponds to non-null potentials associated with a single relative position  $\mathbf{r}$  and we denote by  $d$  the dimension of  $\boldsymbol{\theta}_{\mathbf{r}}$ , which is given by  $d = (|\mathcal{Z}|)^2 - 1$ .

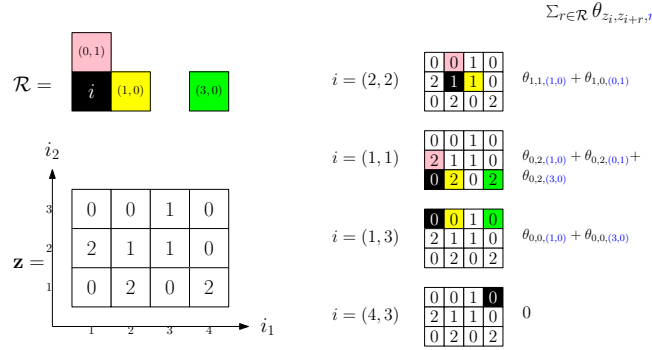


Figure 1: An example field  $\mathbf{z}$  with dimensions  $n_1 = 4$ ,  $n_2 = 3$  and the computed sums  $\sum_{\mathbf{r} \in \mathcal{R}} \theta_{z_{\mathbf{i}}, z_{\mathbf{i}+\mathbf{r}}, \mathbf{r}}$  for some positions  $\mathbf{i}$  considering a RPS  $\mathcal{R} = \{(1,0), (0,1), (3,0)\}$ .

## 2.2 Conditional Probabilities and Pseudolikelihood

While the MRF model introduced is well-defined, inference for such model gets problematic on non-trivial cases due to the intractability of the normalizing constant,  $\zeta(\boldsymbol{\theta})$ , as it requires computing a sum of an exponential number of terms,  $(|\mathcal{Z}|)^{n_1 n_2}$ , which quickly becomes infeasible. For example, even for  $n_1 = n_2 = 100$ , which is not even considered large for common applications, computing the normalizing constant is impractical.

One of the most important features of MRF models is local dependence that makes probability functions decomposable into a product of functions that depend on  $\mathbf{z}$  only through subsets of it, like pairs  $(z_{\mathbf{i}}, z_{\mathbf{i}+\mathbf{r}})$ , in the case of (1). This decomposition allows expressing the conditional probability of specific  $z_{\mathbf{i}}$  given every other element  $\mathbf{z}_{-\mathbf{i}} = \{z_{\mathbf{i}'} : \mathbf{i}' \in \mathcal{S}, \mathbf{i}' \neq \mathbf{i}\}$  as

$$f(z_{\mathbf{i}} | \mathbf{z}_{-\mathbf{i}}, \mathcal{R}, \boldsymbol{\theta}) = f(z_{\mathbf{i}} | \mathbf{z}_{\mathcal{N}_{\mathbf{i}}}, \mathcal{R}, \boldsymbol{\theta}) = \frac{\exp\left(\sum_{\mathbf{r} \in \mathcal{R}} \theta_{z_{\mathbf{i}}, z_{\mathbf{i}+\mathbf{r}}, \mathbf{r}} + \theta_{z_{\mathbf{i}-\mathbf{r}}, z_{\mathbf{i}}, \mathbf{r}}\right)}{\sum_{a \in \mathcal{Z}} \exp\left(\sum_{\mathbf{r} \in \mathcal{R}} \theta_{a, z_{\mathbf{i}+\mathbf{r}}, \mathbf{r}} + \theta_{z_{\mathbf{i}-\mathbf{r}}, a, \mathbf{r}}\right)}, \quad (2)$$

where  $\mathcal{N}_{\mathbf{i}} \subset \mathcal{S}$  denotes the set of neighbors of  $\mathbf{i}$  based on the RPS  $\mathcal{R}$ , i.e.,  $\mathcal{N}_{\mathbf{i}} = \{\mathbf{i}' : \mathbf{i}' \in \mathcal{S} \text{ and } \mathbf{i}' = \mathbf{i} \pm \mathbf{r}, \mathbf{r} \in \mathcal{R}\}$ .

The computationally simple expressions for conditional probabilities on (2) allows the use of alternative functions based on conditional probabilities instead of the joint probability. For problems with high-dimensional dependent data, when conditional probabilities are available and simple, a function widely used as a proxy for the likelihood function is the **pseudolikelihood function** from Besag (1975), defined as the product of conditional probabilities evaluated at the observed values,  $z_{\mathbf{i}}$ ,

$$\tilde{f}(\mathbf{z} | \mathcal{R}, \boldsymbol{\theta}) = \prod_{\mathbf{i} \in \mathcal{S}} f(z_{\mathbf{i}} | \mathbf{z}_{\mathcal{N}_{\mathbf{i}}}, \mathcal{R}, \boldsymbol{\theta}). \quad (3)$$

Note that while the normalizing constant  $\zeta(\boldsymbol{\theta})$  from (1) requires a sum over  $(|\mathcal{Z}|)^{|\mathcal{S}|}$  random field configurations, (3) involves  $|\mathcal{S}|$  normalizing constants that are sums over  $|\mathcal{Z}|$  terms. Thus, the computational cost for evaluating the pseudolikelihood is  $\mathcal{O}(|\mathcal{Z}| \times |\mathcal{S}|)$ , while the exact likelihood function has a cost of order  $\mathcal{O}(|\mathcal{Z}|^{|\mathcal{S}|})$ .

### 3 A Bayesian Framework for Sparse Interaction Structure Selection

In a Bayesian context, unobservable quantities, for example the parameters of a model, are considered unobserved random variables with specific prior distributions defined beforehand. Many Bayesian model selection methodologies extend this concept by assuming that not only a set of real-valued parameters (the vector of free potentials  $\boldsymbol{\theta}$  within the scope of this work) is a vector of random variables, but also the model itself (interpreted as the RPS  $\mathcal{R}$ ) is an unobserved random object with its given prior distribution.

Considering a collection of proper RPSs denoted  $\mathcal{M}$ , we can define a Bayesian system hierarchically by

$$\begin{aligned} \mathcal{R} &\sim q(\mathcal{R}), & \mathcal{R} &\in \mathcal{M}, \\ \boldsymbol{\theta}|\mathcal{R} &\sim \phi(\boldsymbol{\theta}|\mathcal{R}), & \boldsymbol{\theta} &\in \mathbb{R}^{d|\mathcal{R}|}, \\ \mathbf{z}|\mathcal{R}, \boldsymbol{\theta} &\sim f(\mathbf{z}|\mathcal{R}, \boldsymbol{\theta}), & \mathbf{z} &\in \mathcal{Z}^{|\mathcal{S}|}, \end{aligned}$$

where  $q(\mathcal{R})$  is the prior distribution of the RPS,  $\phi(\boldsymbol{\theta}|\mathcal{R})$  is the prior distribution of the parameter vector  $\boldsymbol{\theta}$  given a particular RPS  $\mathcal{R}$  and  $f(\mathbf{z}|\mathcal{R}, \boldsymbol{\theta})$  is the probability function of a MRF as in (1).

Given that the support of  $\mathcal{R}$  represents the sets of interacting positions, a natural choice for the collection of candidate models  $\mathcal{M}$  is the power set of a **maximal RPS**, denoted  $\mathcal{R}_{\max}$ ,

$$\mathcal{M} = \{\mathcal{R}' : \mathcal{R}' \subset \mathcal{R}_{\max}\},$$

which contains  $2^{|\mathcal{R}_{\max}|}$  possible neighborhoods. For simplicity of notation, we shall use  $\boldsymbol{\theta}$  to denote a vector of varying dimension, which indexing is always associated with an interaction structure  $\mathcal{R}$ . The dimension,  $d|\mathcal{R}|$ , and indexing of  $\boldsymbol{\theta} = (\boldsymbol{\theta}_{\mathbf{r}})_{\mathbf{r} \in \mathcal{R}}$  are always implicitly specified as the vector is consistently matched with an interaction structure  $\mathcal{R}$  in every expression. Note that, within this scope, we are referring as a model to the RPS that defines the interaction structure of a MRF. This problem can also be interpreted as a variable selection problem as any vector of interaction coefficients associated with a RPS  $\mathcal{R}$ , with restrictions that  $\boldsymbol{\theta}_{a,b,\mathbf{r}} = 0$  for all  $a, b$  for specific  $\mathbf{r}$ , can also be expressed (in terms of identical likelihood values) to a model excluding  $\mathbf{r}$  from  $\mathcal{R}$ .

In a model selection context, our main interest is to find the marginal posterior distribution of a model  $\pi(\mathcal{R}|\mathbf{z})$ , which can be obtained by integrating the

(complete) posterior distribution,

$$\pi(\mathcal{R}, \boldsymbol{\theta}|\mathbf{z}) = \frac{q(\mathcal{R})\phi(\boldsymbol{\theta}|\mathcal{R})f(\mathbf{z}|\mathcal{R}, \boldsymbol{\theta})}{\sum_{\mathcal{R}' \in \mathcal{M}} q(\mathcal{R}') \int_{\mathbb{R}^{d|\mathcal{R}'|}} \phi(\boldsymbol{\theta}'|\mathcal{R}')f(\mathbf{z}|\mathcal{R}', \boldsymbol{\theta}')d\boldsymbol{\theta}'}, \quad (4)$$

with respect to  $\boldsymbol{\theta}$ .

Two main computational challenges arise from (4) making most direct analyses prohibitively complex: (I)  $f(\mathbf{z}|\mathcal{R}, \boldsymbol{\theta})$  cannot be evaluated directly due to the intractable normalizing constant and (II) the denominator involves  $2^{|\mathcal{M}|}$  integrations, possibly including many high-dimensional functions that have intractable normalizing constants. Because of these two sources of intractability, this type of posterior distribution is often referred in the literature as a doubly-intractable distribution (Murray et al., 2012; Caimo and Mira, 2015).

Monte Carlo Markov Chain methods are used to generate an ergodic Markov Chain which invariant distribution is equal to a specific target distribution which, in most cases, is a posterior distribution with intractable normalizing constant like (4). Consider an ergodic Markov chain in the space that is a product of  $\mathcal{M}$  by the space of real vectors with varying dimension directly associated with the element of  $\mathcal{M}$ , i.e.,  $(\mathcal{R}^{(1)}, \boldsymbol{\theta}^{(1)}), (\mathcal{R}^{(2)}, \boldsymbol{\theta}^{(2)}), \dots$ , such that  $\boldsymbol{\theta}^{(t)} \in \mathbb{R}^{d|\mathcal{R}^{(t)}|}$ , and invariant measure  $\pi(\cdot, \cdot|\mathbf{z})$ . Then, due to the ergodic theorem, for any bounded function  $g$  of the form

$$g : \mathcal{M} \times \bigcup_{k=0}^{|\mathcal{R}_{\max}|} \mathbb{R}^{dk} \rightarrow \mathbb{R},$$

we have

$$\sum_{t=1}^n g(\mathcal{R}^{(t)}, \boldsymbol{\theta}^{(t)}) \rightarrow \mathbb{E}_{\pi}(g(\mathcal{R}, \boldsymbol{\theta})|\mathbf{z}), \quad \text{a.s.} \quad (5)$$

where  $\mathbb{E}_{\pi}(g(\mathcal{R}, \boldsymbol{\theta})|\mathbf{z})$  is the conditional expected value of the random variable  $g(\mathcal{R}, \boldsymbol{\theta})$  given the observed  $\mathbf{z}$ , under the (target) distribution  $\pi(\mathcal{R}, \boldsymbol{\theta}|\mathbf{z})$ . Some particular choices of  $g$  lead to interpretable quantities, that are useful for evaluating the plausibility of interaction neighborhoods  $\mathcal{R}$  based on their posterior distribution, such as  $g(\mathcal{R}, \boldsymbol{\theta}) = \mathbb{1}(\mathcal{R} = \mathcal{R}^*)$ , which results in (5) being the posterior probability of a particular neighborhood  $\mathcal{R}^*$  or  $g(\mathcal{R}, \boldsymbol{\theta}) = \mathbb{1}(\mathbf{r} \in \mathcal{R})$ , which corresponds to the marginal posterior probability that a particular relative position  $\mathbf{r}$  belongs to the RPS.

Given the estimated marginal posterior probabilities for each position in  $\mathcal{R}_{\max}$ , obtained from a Metropolis-Hastings sample of size  $T$ , and a threshold value  $c_{\text{th}}$ , a sparse estimator of the RPS, denoted  $\hat{\mathcal{R}}_{\text{sp}}(c_{\text{th}})$ , can be obtained by selecting the set of all positions with (estimated) posterior probability exceeding  $c_{\text{th}}$ ,

$$\hat{\mathcal{R}}_{\text{sp}}(c_{\text{th}}) = \{\mathbf{r} \in \mathcal{R}_{\max} : \frac{1}{T} \sum_{t=1}^T \mathbb{1}(\mathbf{r} \in \mathcal{R}^{(t)}) > c_{\text{th}}\}. \quad (6)$$

### 3.1 Pseudoposterior-based inference

In order to overcome the computational infeasibility due to the intractable normalizing constant of the likelihood function  $f$  defined in (1), many methods for inference on MRFs have been proposed. One of the commonly used approaches is to replace the likelihood function,  $f$ , for the pseudolikelihood,  $\tilde{f}$ , defined in (3), which can be evaluated directly.

When applied to the Bayesian system defined in the previous section, this replacement of the likelihood function leads to an alternative function referred as pseudoposterior distribution, that is proportional to the product of prior distributions and the pseudolikelihood, and it is formally defined as (*cf.* with (4))

$$\tilde{\pi}(\mathcal{R}, \boldsymbol{\theta}|\mathbf{z}) = \frac{q(\mathcal{R})\phi(\boldsymbol{\theta}|\mathcal{R})\tilde{f}(\mathbf{z}|\mathcal{R}, \boldsymbol{\theta})}{\sum_{\mathcal{R}' \in \mathcal{M}} q(\mathcal{R}') \int_{\mathbb{R}^{d|\mathcal{R}'|}} \phi(\boldsymbol{\theta}'|\mathcal{R}')\tilde{f}(\mathbf{z}|\mathcal{R}', \boldsymbol{\theta}')d\boldsymbol{\theta}'}. \quad (7)$$

It is valuable to note that, while the pseudolikelihood is a plausible proxy for the likelihood function in terms of optimization-related mathematical properties, these functions may have different overall shapes depending on how much dependence exists on the dataset considered, and composing functions using the pseudolikelihood instead of the likelihood alters how these functions are interpreted. As a consequence, Bayesian inference based on pseudoposterior produces useful quantities, but the information obtained cannot be interpreted in the conventional way. For example, integrating the pseudoposterior distribution over  $\boldsymbol{\theta}$  does not result exactly in the posterior distribution of the RPSs  $\mathcal{R}$ , but a different measure conceivably useful for evaluating the plausibility of the RPSs.

### 3.2 A Reversible Jump Proposal Kernel for Sparse Neighborhood Detection

Constructing a proposal kernel for the Metropolis-Hastings algorithm that can efficiently move through both the model space  $\mathcal{M}$  and the space of interaction coefficients within a model is not a simple task. Green (1995) proposes the Reversible Jump Monte Carlo Markov Chain (RJMCMC) as a framework for Bayesian analysis of models and varying dimension parameters simultaneously. In general, the strategy consists of composing a proposal kernel which is a mixture of simpler kernels, some proposing within-model moves that only changes parameter values and others proposing reversible jumps between models that have good analytical or computational properties.

In this work, we construct a customized proposal kernel for the model inspired on properties and examples from Brooks et al. (2003) with additional features that are specifically designed for neighborhood selection for MRFs. This proposal kernel consists of a mixture of 4 types of moves seeking to come up with states that might have higher pseudoposterior density than the current state with some probability.

**Within-model random walk.** The first and simplest move consists of adding a random walk term to the current value of the parameter vector. Given a current pair  $(\mathcal{R}, \boldsymbol{\theta})$ , we keep the same neighborhood,  $\mathcal{R}' = \mathcal{R}$ , and propose a new vector of interaction coefficients  $\boldsymbol{\theta}' \in \mathcal{Z}^{d|\mathcal{R}|}$  by adding a Gaussian noise term with matching dimension, each coordinate being independent and identically distributed with mean 0 and variance  $\sigma_w^2$ , where  $\sigma_w^2$  is a tuning parameter of the algorithm.

The transition kernel density for this move is given by

$$\kappa_w(\boldsymbol{\theta}', \mathcal{R}' | \boldsymbol{\theta}, \mathcal{R}) = \frac{1}{(2\pi\sigma_w^2)^{d|\mathcal{R}|/2}} \exp\left(-\frac{1}{2\sigma_w^2} \sum_{\mathbf{r} \in \mathcal{R}} (\boldsymbol{\theta}_{\mathbf{r}} - \boldsymbol{\theta}'_{\mathbf{r}})^\top (\boldsymbol{\theta}_{\mathbf{r}} - \boldsymbol{\theta}'_{\mathbf{r}})\right) \mathbf{1}(\mathcal{R}' = \mathcal{R}),$$

making this proposal density not only reversible, but also symmetrical, i.e.,  $\kappa_w(\boldsymbol{\theta}', \mathcal{R}' | \boldsymbol{\theta}, \mathcal{R}) = \kappa_w(\boldsymbol{\theta}, \mathcal{R} | \boldsymbol{\theta}', \mathcal{R}')$ . Since proposed states keep the same interaction structure, we also have  $q(\mathcal{R}) = q(\mathcal{R}')$ , so the terms corresponding to the neighborhood interaction structure are also cancelled in the acceptance ratio.

While this move does not contribute to jumping between RPSs, its goal is to add small incremental changes in the parameter coordinates so that the chain gradually moves towards higher pseudoposterior density regions within a model. Typically, small values of  $\sigma_w^2$  are preferred so that the coefficients within a RPS are slowly drifting towards the maximum pseudoposterior vector for that RPS.

**Birth and Death.** We propose a jump move from a state  $(\mathcal{R}, \boldsymbol{\theta})$  to a state  $(\mathcal{R}', \boldsymbol{\theta}')$ ,  $\mathcal{R}' \neq \mathcal{R}$ , by either including a position from  $\mathcal{R}_{\max}$  that is not already in  $\mathcal{R}$ , or by removing one of the positions in  $\mathcal{R}$ . We refer to these moves as Birth and Death of a relative position, respectively.

We define the RPS comparison operator  $\overset{\mathbf{r}}{\prec}$  as

$$\mathcal{R} \overset{\mathbf{r}}{\prec} \mathcal{R}' \iff \mathcal{R} \subset \mathcal{R}', \mathbf{r} \notin \mathcal{R} \text{ and } \mathcal{R} \cup \{\mathbf{r}\} = \mathcal{R}',$$

which means that  $\mathcal{R}'$  can be obtained by adding the position  $\mathbf{r}$  to  $\mathcal{R}$ . Given a current RPS  $\mathcal{R}$ , we randomly select a position  $\mathbf{r}^*$  from  $\mathcal{R}_{\max}$  with uniform probabilities  $\frac{1}{|\mathcal{R}_{\max}|}$ . Then either a birth or death move is proposed depending on the selected  $\mathbf{r}^*$ .

- If  $\mathbf{r}^* \in \mathcal{R}$ , the proposed RPS  $\mathcal{R}'$  is such that  $\mathcal{R}' \overset{\mathbf{r}^*}{\prec} \mathcal{R}$ , i.e.,  $\mathbf{r}^*$  is removed from  $\mathcal{R}$ . For the associated interaction coefficients  $\boldsymbol{\theta}'$  to be proposed with  $\mathcal{R}'$ , all the values are kept the same  $\boldsymbol{\theta}'_{\mathbf{r}} = \boldsymbol{\theta}_{\mathbf{r}}$  for  $\mathbf{r} \in \mathcal{R}'$ .
- If  $\mathbf{r}^* \notin \mathcal{R}$ ,  $\mathcal{R}'$  is proposed by including  $\mathbf{r}^*$ , i.e.,  $\mathcal{R} \overset{\mathbf{r}^*}{\prec} \mathcal{R}'$ . For the proposed parameter  $\boldsymbol{\theta}'$ , we keep the values of the previous  $\boldsymbol{\theta}'_{\mathbf{r}} = \boldsymbol{\theta}_{\mathbf{r}}$  for the previously included positions  $\mathbf{r} \in \mathcal{R}$  and sample a new vector of i.i.d. Gaussian variables with mean 0 and variance  $\sigma_{\text{bd}}^2$  to assign to  $\boldsymbol{\theta}'_{\mathbf{r}^*}$ .

Note that, by this definition, transitions between states with two different RPSs  $\mathcal{R}$  and  $\mathcal{R}'$  are allowed if, and only if,  $|\mathcal{R} \nabla \mathcal{R}'| = 1$ , where  $\nabla$  denotes the symmetrical difference operator for two sets. Therefore, the proposal kernel density for

a birth/death jump move is given by

$$\kappa_{\text{bd}}(\boldsymbol{\theta}', \mathcal{R}' | \boldsymbol{\theta}, \mathcal{R}) = \begin{cases} \frac{1}{|\mathcal{R}_{\text{max}}|} \frac{\exp\left(-\frac{1}{2\sigma_{\text{bd}}^2} \boldsymbol{\theta}'_{\mathbf{r}^*} \boldsymbol{\theta}'_{\mathbf{r}^*}\right)}{(2\pi\sigma_{\text{bd}}^2)^{d/2}} \prod_{\mathbf{r} \in \mathcal{R}} \mathbb{1}(\boldsymbol{\theta}'_{\mathbf{r}} = \boldsymbol{\theta}_{\mathbf{r}}) & , \text{ if } \mathcal{R} \prec_{\mathbf{r}^*} \mathcal{R}', \\ \frac{1}{|\mathcal{R}_{\text{max}}|} \prod_{\mathbf{r} \in \mathcal{R}'} \mathbb{1}(\boldsymbol{\theta}'_{\mathbf{r}} = \boldsymbol{\theta}_{\mathbf{r}}) & , \text{ if } \mathcal{R}' \prec_{\mathbf{r}^*} \mathcal{R}, \\ 0 & , \text{ if } |\mathcal{R} \nabla \mathcal{R}'| \neq 1. \end{cases}$$

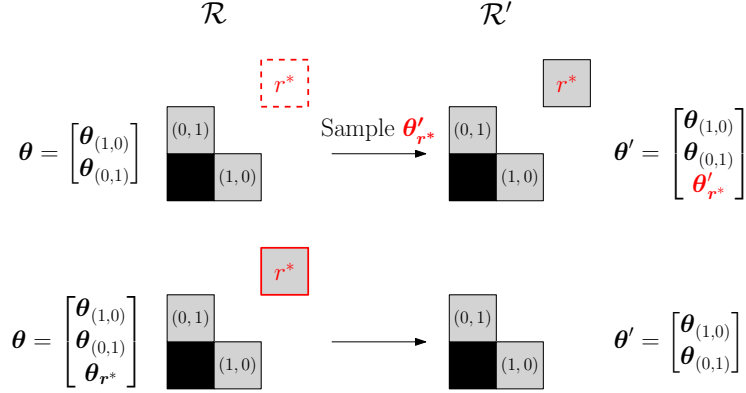


Figure 2: Illustration of a Birth/Death Jump proposal when sampling  $\mathbf{r}^* \notin \mathcal{R}$  (top) and  $\mathbf{r}^* \in \mathcal{R}$  (bottom).

Figure 2 illustrates how new states  $(\mathcal{R}', \boldsymbol{\theta}')$  are proposed from a current  $(\mathcal{R}, \boldsymbol{\theta})$  when a randomly selected position  $\mathbf{r}^*$  is included or not included in  $\mathcal{R}$ . It is straightforward to conclude from the example that this type of jump can be reversed by selecting the same position  $\mathbf{r}^*$  and, the case of adding a new position, sampling the appropriate  $\boldsymbol{\theta}'_{\mathbf{r}^*}$ , therefore,  $\kappa_{\text{bd}}(\boldsymbol{\theta}', \mathcal{R}' | \boldsymbol{\theta}, \mathcal{R}) > 0$  if, and only if,  $\kappa_{\text{bd}}(\boldsymbol{\theta}, \mathcal{R} | \boldsymbol{\theta}', \mathcal{R}') > 0$ .

**Position swap.** As second type of move constructed for proposing jumps between states with different RPS is to swap one of positions in the current RPS,  $\mathbf{r}_{\text{in}} \in \mathcal{R}$ , for another one  $\mathbf{r}_{\text{out}} \in \mathcal{R}_{\text{max}} \setminus \mathcal{R}$ , while keeping all of the interaction coefficients the same, including the subvector associated with the swapped position,  $\boldsymbol{\theta}'_{\mathbf{r}_{\text{out}}} = \boldsymbol{\theta}_{\mathbf{r}_{\text{in}}}$ . Figure 3 illustrates an example of the position swap move.

The positions  $\mathbf{r}_{\text{in}}$  and  $\mathbf{r}_{\text{out}}$ , for the swap move, are chosen independently and uniformly distributed on  $\mathcal{R}$  and  $\mathcal{R}_{\text{max}} \setminus \mathcal{R}$ , respectively. Therefore, for any states  $(\boldsymbol{\theta}, \mathcal{R})$  and  $(\boldsymbol{\theta}', \mathcal{R}')$  such that  $|\mathcal{R}| = |\mathcal{R}'|$  and  $|\mathcal{R} \nabla \mathcal{R}'| = 2$ , differing only in the presence of relative positions  $\mathbf{r}_{\text{in}} \in \mathcal{R}$  and  $\mathbf{r}_{\text{out}} \in \mathcal{R}'$ , the proposal density for the swap move is given by

$$\kappa_{\text{sw}}(\boldsymbol{\theta}', \mathcal{R}' | \boldsymbol{\theta}, \mathcal{R}) = \frac{1}{|\mathcal{R}| |\mathcal{R}_{\text{max}} \setminus \mathcal{R}|} \prod_{\mathbf{r} \in \mathcal{R} \cap \mathcal{R}'} \mathbb{1}(\boldsymbol{\theta}_{\mathbf{r}} = \boldsymbol{\theta}'_{\mathbf{r}}) \mathbb{1}(\boldsymbol{\theta}_{\mathbf{r}_{\text{in}}} = \boldsymbol{\theta}'_{\mathbf{r}_{\text{out}}}). \quad (8)$$

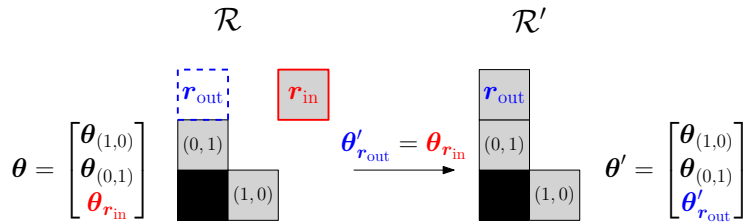


Figure 3: Illustration of a Position swap move proposal.

Note that (8) is a symmetrical kernel since the inverse operation is proposed by selecting the same pair of positions  $\mathbf{r}_{\text{in}}$  and  $\mathbf{r}_{\text{out}}$  reversed, the RPS prior probability only depends on the size of the current RPS,  $|\mathcal{R}|$ , and we have the condition that  $|\mathcal{R}| = |\mathcal{R}'|$  for every pair of states with positive proposal probability.

The rationale behind this move is that, due to the spatial dependence intrinsic to lattice-based indexing of the MRF model considered, the counts of pairwise configurations in some relative positions may present high correlation, especially when those relative positions are close (e.g.  $\mathbf{r}$  and  $\mathbf{r} + (1, 0)$ ) or a multiple one from another (e.g.  $\mathbf{r}$  and  $2\mathbf{r}$ ).

Note that while the same jumps proposed by swap moves could be achieved by a series of birth and death moves, one of those steps would be to exclude a relative position,  $\mathbf{r}_{\text{in}}$ , with associated interaction coefficient,  $\theta_{\mathbf{r}_{\text{in}}}$ , possibly far from the zero vector, what would cause the acceptance of such move to be highly unlikely. Thus, swap moves is a proposal step that avoids the algorithm getting stuck at a local (with respect to RPSs) maxima, by adding direct connections to states with different RPSs that may have similar pseudoposterior values, taking into account very specific characteristics of the model.

**Split and Merge.** While the position swap move is proposed in order to allow a relative position included in a state to be substituted by another one that is not included but has a similar pseudoposterior value, another type of local maxima may exist when two or more relative positions with highly correlated sufficient statistics are included in a model simultaneously.

The correlation between vectors of sufficient statistics may cause interaction weights for some relative positions  $\theta_{\mathbf{r}}$  to become very unstable, due to the possibility of compensating shifts in one direction for one of the vectors with equivalent shifts in the opposite direction.

We define the Split and Merge moves as a pair of reversible operations that not only allow jumps between different RPSs but also control the values of  $\theta_{\mathbf{r}}$  involved. This transition has the goal of redistributing the interactions coefficients, allowing smaller or larger RPSs with similar likelihood to be proposed with some probability. The Merge move permits excessive relative positions to be removed from the current state and possibly generates a proposed state that distributes the interaction weights  $\theta_{\mathbf{r}}$  of the position to be removed, by adding

it to the remaining positions, hopefully keeping the pseudolikelihood values on similar levels. The key premise on this pair of moves is that, for a pair of states  $(\mathcal{R}, \boldsymbol{\theta})$  and  $(\mathcal{R}', \boldsymbol{\theta}')$ , we have

$$\sum_{\mathbf{r} \in \mathcal{R}} \boldsymbol{\theta}_{\mathbf{r}} = \sum_{\mathbf{r} \in \mathcal{R}'} \boldsymbol{\theta}'_{\mathbf{r}}.$$

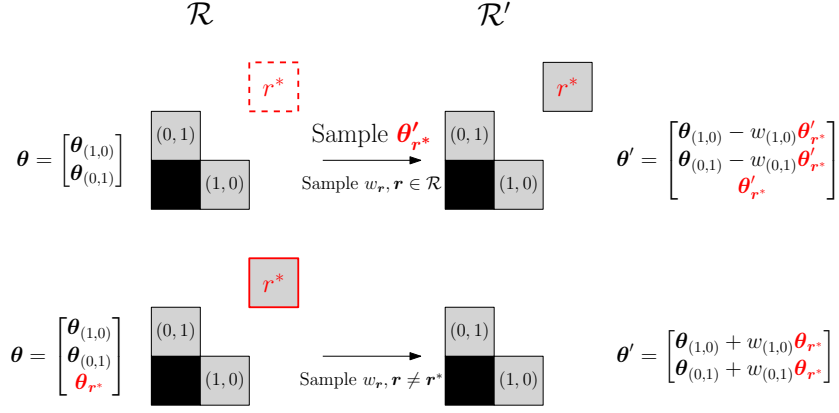


Figure 4: Illustration of Split (top) and Merge (bottom) moves.

Given a current state  $(\mathcal{R}, \boldsymbol{\theta})$ , the process of proposing a state  $(\mathcal{R}', \boldsymbol{\theta}')$  with a **Split** move is composed by the steps of

1. Sample a new position  $\mathbf{r}^*$  to be included from  $\mathcal{R}_{\max} \setminus \mathcal{R}$  with uniform probability.
2. Generate a new interaction coefficient vector  $\boldsymbol{\theta}'_{\mathbf{r}^*}$  from a  $d$ -dimensional independent Gaussian distribution with variances  $\sigma_s^2$ , where the split variance,  $\sigma_s^2$ , is a tuning parameter of the algorithm.
3. Generate a vector of weights  $\mathbf{w} = (w_r)_{r \in \mathcal{R}}$  from a symmetric Dirichlet distribution with all parameters equal to  $\nu$ , where  $\nu$  is another tuning parameter of the algorithm. Lower values for  $\nu$  can be used in order to “concentrate” the weights sampled from the Dirichlet distribution within few positions when proposing a Split move.
4. Propose  $\mathcal{R}' = \mathcal{R} \cup \mathbf{r}^*$  and  $\boldsymbol{\theta}'$  such that  $\boldsymbol{\theta}'_{\mathbf{r}^*}$  is the generated vector and  $\boldsymbol{\theta}'_{\mathbf{r}} = \boldsymbol{\theta}_{\mathbf{r}} - w_{\mathbf{r}} \boldsymbol{\theta}'_{\mathbf{r}^*}$  for every other relative position  $\mathbf{r} \in \mathcal{R}$ .

The proposal density for a Split move,  $\kappa_s$ , is given by

$$\begin{aligned} \kappa_s(\boldsymbol{\theta}', \mathcal{R}' | \boldsymbol{\theta}, \mathcal{R}) &= \frac{\prod_{\mathbf{r}^* \in \mathcal{R}_{\max} \setminus \mathcal{R}} \mathbb{1}(\mathcal{R} \stackrel{\mathbf{r}^*}{\prec} \mathcal{R}') \exp\left(\frac{-(\boldsymbol{\theta}'_{\mathbf{r}^*} \top \boldsymbol{\theta}_{\mathbf{r}^*})}{2\sigma_s^2}\right)}{|\mathcal{R}_{\max} \setminus \mathcal{R}| (2\pi\sigma_s^2)^{d/2}} \\ &\quad \frac{\Gamma(|\mathcal{R}| \nu)}{\prod_{\mathbf{r} \in \mathcal{R}} (\Gamma(\nu))} \prod_{\mathbf{r} \in \mathcal{R}} \left[ \left( \frac{\theta_{0,1,\mathbf{r}} - \theta'_{0,1,\mathbf{r}}}{\theta'_{0,1,\mathbf{r}^*}} \right)^{\nu-1} \times \frac{\mathbb{1}\left(0 < \frac{\theta_{0,1,\mathbf{r}} - \theta'_{0,1,\mathbf{r}}}{\theta'_{0,1,\mathbf{r}^*}} < 1\right)}{\theta'_{0,1,\mathbf{r}^*}} \right] \\ &\quad \mathbb{1}\left(\sum_{\mathbf{r} \in \mathcal{R}} (\boldsymbol{\theta}_{\mathbf{r}} - \boldsymbol{\theta}'_{\mathbf{r}}) = \boldsymbol{\theta}'_{\mathbf{r}^*}\right) \prod_{a,b \in \mathcal{Z}^2} \mathbb{1}\left(\frac{\theta_{a,b,\mathbf{r}} - \theta'_{a,b,\mathbf{r}}}{\theta'_{a,b,\mathbf{r}^*}} = \frac{\theta_{0,1,\mathbf{r}} - \theta'_{0,1,\mathbf{r}}}{\theta'_{0,1,\mathbf{r}^*}}\right). \end{aligned}$$

The **Merge** proposal move is the reverse of the Split move and can be described by the following sequence of steps

1. Sample a state  $\mathbf{r}^*$  from  $\mathcal{R}$ , which interaction coefficient vector will be merged into the others, with uniform probabilities.
2. Generate a vector of weights  $\mathbf{w} = (w_{\mathbf{r}})_{\mathbf{r} \in (\mathcal{R} \setminus \mathbf{r}^*)}$  with Dirichlet distribution with all parameters equal to  $\nu$ .
3. Propose  $\mathcal{R}' = \mathcal{R} \setminus \mathbf{r}^*$  and  $\boldsymbol{\theta}'$  such that  $\boldsymbol{\theta}'_{\mathbf{r}} = \boldsymbol{\theta}_{\mathbf{r}} + w_{\mathbf{r}} \boldsymbol{\theta}_{\mathbf{r}^*}$  for each  $\mathbf{r} \in \mathcal{R}'$ .

The proposal density for a Merge move is

$$\begin{aligned} \kappa_m(\boldsymbol{\theta}', \mathcal{R}' | \boldsymbol{\theta}, \mathcal{R}) &= \frac{\prod_{\mathbf{r}^* \in \mathcal{R}} \mathbb{1}(\mathcal{R}' \stackrel{\mathbf{r}^*}{\prec} \mathcal{R})}{|\mathcal{R}|} \\ &\quad \frac{\Gamma(|\mathcal{R}'| \nu)}{\prod_{\mathbf{r} \in \mathcal{R}'} (\Gamma(\nu))} \prod_{\mathbf{r} \in \mathcal{R}'} \left[ \left( \frac{\theta'_{0,1,\mathbf{r}} - \theta_{0,1,\mathbf{r}}}{\theta_{0,1,\mathbf{r}^*}} \right)^{\nu-1} \times \frac{\mathbb{1}\left(0 < \frac{\theta'_{0,1,\mathbf{r}} - \theta_{0,1,\mathbf{r}}}{\theta_{0,1,\mathbf{r}^*}} < 1\right)}{\theta_{0,1,\mathbf{r}^*}} \right] \\ &\quad \mathbb{1}\left(\sum_{\mathbf{r} \in \mathcal{R}'} \boldsymbol{\theta}'_{\mathbf{r}} - \boldsymbol{\theta}_{\mathbf{r}} = \boldsymbol{\theta}_{\mathbf{r}^*}\right) \prod_{a,b \in \mathcal{Z}^2} \mathbb{1}\left(\frac{\theta_{a,b,\mathbf{r}} - \theta'_{a,b,\mathbf{r}}}{\theta'_{a,b,\mathbf{r}^*}} = \frac{\theta_{0,1,\mathbf{r}} - \theta'_{0,1,\mathbf{r}}}{\theta'_{0,1,\mathbf{r}^*}}\right). \end{aligned}$$

It is easy to see that an accepted Split move is reversed by a Merge move if the sampled relative position  $\mathbf{r}^*$  and the generated vector of weights  $\mathbf{w}$  is the same for both moves. This fact also produces an analytical simplification in the ratio of proposal densities, required for computing the acceptance ratio in the Metropolis-Hastings algorithm, for these moves as

$$\frac{\kappa_m(\boldsymbol{\theta}, \mathcal{R} | \boldsymbol{\theta}', \mathcal{R}')}{\kappa_s(\boldsymbol{\theta}', \mathcal{R}' | \boldsymbol{\theta}, \mathcal{R})} = \frac{|\mathcal{R}_{\max} \setminus \mathcal{R}| \exp\left(\frac{-(\boldsymbol{\theta}'_{\mathbf{r}^*} \top \boldsymbol{\theta}_{\mathbf{r}^*})}{2\sigma_s^2}\right)}{|\mathcal{R}'| (2\pi\sigma_s^2)^{d/2}}, \quad (9)$$

for any pair of states  $(\mathcal{R}, \boldsymbol{\theta})$  and  $(\mathcal{R}', \boldsymbol{\theta}')$  such that  $\kappa_s(\boldsymbol{\theta}', \mathcal{R}' | \boldsymbol{\theta}, \mathcal{R}) > 0$ . The ratio of proposal densities for the reversed transitions can be achieved by applying the inverse of (9).

**Mixture proposal density.** Each move described previously has a different goal in terms of how a region (in terms of both RPS and interaction coefficients) of much higher posterior density could be proposed with some probability improving the rate of convergence of the Metropolis-Hastings algorithm to a region corresponding to a global maximum. In order to assemble the five groups of moves into a single transition kernel, we define a proposal density  $\kappa$  that is composed by a mixture of the of five described densities

$$\kappa(\boldsymbol{\theta}', \mathcal{R}' | \boldsymbol{\theta}, \mathcal{R}) = \sum_{\Psi \in \{\text{w, bd, sw, m, s}\}} p_{\Psi}(\mathcal{R}) \kappa_{\Psi}(\boldsymbol{\theta}', \mathcal{R}' | \boldsymbol{\theta}, \mathcal{R}), \quad (10)$$

where  $p_{\Psi}(\mathcal{R})$  corresponds to the probability of selecting a move  $\Psi$  when the current state has the RPS component as  $\mathcal{R}$  and  $\sum_{\Psi} p_{\Psi}(\mathcal{R}) = 1$ . Having the mixture probabilities depend on the current RPS is required to avoid undefined behaviors such as proposing a random walk move  $\kappa_{\text{w}}$  when we have an empty RPS,  $\mathcal{R} = \emptyset$ .

Following [Green \(1995\)](#) and [Brooks et al. \(2003\)](#), we can describe the acceptance of the Metropolis-Hastings (Reversible Jump) algorithm when using a mixture proposal density by using the ratio of the sampled move  $\Psi$  at each step,

$$\mathcal{A}_{\Psi}(\boldsymbol{\theta}', \mathcal{R}' | \boldsymbol{\theta}, \mathcal{R}) = \frac{q(\mathcal{R}')}{q(\mathcal{R})} \frac{\pi(\boldsymbol{\theta}' | \mathcal{R}')}{\pi(\boldsymbol{\theta} | \mathcal{R})} \frac{\tilde{f}(\boldsymbol{\theta}', \mathcal{R}')}{\tilde{f}(\boldsymbol{\theta}, \mathcal{R})} \frac{p_{\Psi'}(\mathcal{R})}{p_{\Psi}(\mathcal{R})} \frac{\kappa_{\Psi'}(\boldsymbol{\theta}, \mathcal{R} | \boldsymbol{\theta}', \mathcal{R}')}{\kappa_{\Psi}(\boldsymbol{\theta}', \mathcal{R}' | \boldsymbol{\theta}, \mathcal{R})}, \quad (11)$$

where  $\Psi'$  is the inverse move of the move  $\Psi$ , i.e.,  $\Psi' = \Psi$  if  $\Psi = \text{w, bd}$  or  $\text{sw}$  and swapped for  $\Psi = \text{s}$  or  $\text{m}$ . The complete procedure is described in [Algorithm 1](#). In practice, computations involving  $\mathcal{A}_{\Psi}(\cdot, \cdot | \cdot, \cdot)$  can be performed in logarithmic scale for both analytical and numerical simplicity.

---

**Algorithm 1:** Metropolis-Hastings algorithm with mixture proposal density.

---

```

Set the initial state  $(\mathcal{R}^{(0)}, \boldsymbol{\theta}^{(0)})$ ;
foreach  $t = 0, \dots, n_{iter}$  do
    Sample a random move  $\Psi$  from  $\{\text{w, bd, sw, s, m}\}$  with probabilities
     $p_{\text{w}}(\mathcal{R}^{(t)}), p_{\text{bd}}(\mathcal{R}^{(t)}), p_{\text{sw}}(\mathcal{R}^{(t)}), p_{\text{s}}(\mathcal{R}^{(t)}), p_{\text{m}}(\mathcal{R}^{(t)})$ ;
    Propose a new state  $(\mathcal{R}', \boldsymbol{\theta}')$  by sampling from the proposal density
     $\kappa_{\Psi}(\cdot, \cdot | \mathcal{R}^{(t)}, \boldsymbol{\theta}^{(t)})$ ;
    Compute the Acceptance Ratio  $\mathcal{A}(\mathcal{R}', \boldsymbol{\theta}' | \mathcal{R}^{(t)}, \boldsymbol{\theta}^{(t)})$  from (11);
    if  $U < \mathcal{A}(\mathcal{R}', \boldsymbol{\theta}' | \mathcal{R}^{(t)}, \boldsymbol{\theta}^{(t)})$  then
        |  $(\mathcal{R}^{(t+1)}, \boldsymbol{\theta}^{(t+1)}) \leftarrow (\mathcal{R}', \boldsymbol{\theta}')$ 
    else
        |  $(\mathcal{R}^{(t+1)}, \boldsymbol{\theta}^{(t+1)}) \leftarrow (\mathcal{R}^{(t)}, \boldsymbol{\theta}^{(t)})$ 

```

---

### 3.3 Prior Distributions Specification

An important element of Bayesian Inference is the choice of prior distributions for the unobserved quantities. Although these distributions are meant to reflect previous information that can be incorporated in the model, their general forms are often restricted to specific families with good analytical and computational properties, while still preserving some flexibility to include prior information in the form of hyper-parameters which may have useful interpretations depending on the chosen family of prior distributions.

The prior distribution of the RPS,  $q(\mathcal{R})$ , can be freely specified according to the application and previous information being considered. However, in this work, for simplicity, we consider  $q(\mathcal{R})$  to be constant (uniform distribution). This choice will simplify both the computation of the acceptance probabilities and the incorporation of application-specific information. Other choices of prior distributions could involve functions that penalize  $\mathcal{R}$  by  $|\mathcal{R}|$  or penalize individual positions (e.g., long-range relative positions reduce the probability of an RPS). However, these choices would require problem-specific knowledge and could make the computation of acceptance ratios more complex.

For the prior distribution of  $\boldsymbol{\theta}$  given a RPS,  $\phi(\boldsymbol{\theta}|\mathcal{R})$ , a standard choice is to use independent normal distributions, with a given fixed prior variance,  $\sigma_p^2$ , and zero mean, i.e.,

$$\phi(\boldsymbol{\theta}|\mathcal{R}) = \frac{1}{(2\pi\sigma_p^2)^{|\mathcal{R}|d/2}} \exp\left(-\frac{1}{2\sigma_p^2} \sum_{\mathbf{r} \in \mathcal{R}} \boldsymbol{\theta}_{\mathbf{r}}^\top \boldsymbol{\theta}_{\mathbf{r}}\right). \quad (12)$$

One of the main advantages of this prior distribution is that ratios,  $\phi(\boldsymbol{\theta}|\mathcal{R})/\phi(\boldsymbol{\theta}'|\mathcal{R}')$ , used for computing acceptance ratios of the RJMCMC algorithm described previously, can be computed more efficiently due to advantages from good analytical properties. For example, the ratio is always 1 for Position Swap moves and the density (or the inverse of) of a  $d$ -dimensional Normal distribution for Birth and Death moves. Since those computations are carried in logarithmic scale, most of the terms involving  $\boldsymbol{\theta}$  will be sums of quadratic forms that are simple to evaluate.

## 4 Simulation Study

In order to validate the practical use of the proposed RJMCMC algorithm and understand the effect of the RPS prior distribution choice on the selected models, we conducted a simulation study where three MRFs on a  $150 \times 150$  lattice,  $\mathbf{Z}^{(i)}$ , were simulated using sparse interaction structures  $\mathcal{R}^{(i)}$ ,  $i = 1, 2, 3$ , and alphabet  $\mathcal{Z} = \{0, 1, 2\}$ . The sparse RPSs considered have increasing complexity and are specified as follows:

- $\mathcal{R}_1 = \{(1, 0), (0, 1)\}$ ,
- $\mathcal{R}_2 = \{(1, 0), (0, 1), (3, 3)\}$ ,

- $\mathcal{R}_3 = \{(1, 0), (0, 1), (3, 3), (2, 0)\}$ ,

and for the maximal RPS we considered  $\mathcal{R}_{\max}$  containing all relative positions within a maximum distance of 5 from the origin, excluding positions that are the opposite of another one included to ensure that it is a proper RPS, as illustrated in Figure 5.



Figure 5: Interaction structures considered in simulations  $\mathcal{R}_i$ ,  $i = 1, 2, 3$  and maximal interaction structure  $\mathcal{R}_{\max}$  considered in the reversible jump algorithm.

With  $|\mathcal{Z}| = 3$ , a total of  $d = 8$  coefficients may vary for each relative position  $\mathbf{r}$ , therefore,  $\mathcal{R}_{\max}$ , which has a total of 60 positions, is associated with 480 free interaction coefficients when every relative position is included, whereas  $\mathcal{R}_3$ , the most complex of the three RPSs that generated the data, represents a model with 32 free interaction coefficients. This reduction from 480 to 32 (or less) free quantities in a model may be extremely useful for inference by reducing complexity and computational cost, as long as the interactions, within the selected set of relative positions, can capture most of the dependence structure of the data.

We considered the same interaction coefficients  $\theta_{a,b,\mathbf{r}}$  across simulations for each position  $\mathbf{r}$  with values described in Table 1 and the simulated observations are presented in Figure 6. The coefficient values were selected to generate different patterns in the sampled images and it is not intuitively clear, which set of relative position best describes the patterns generated in each image.

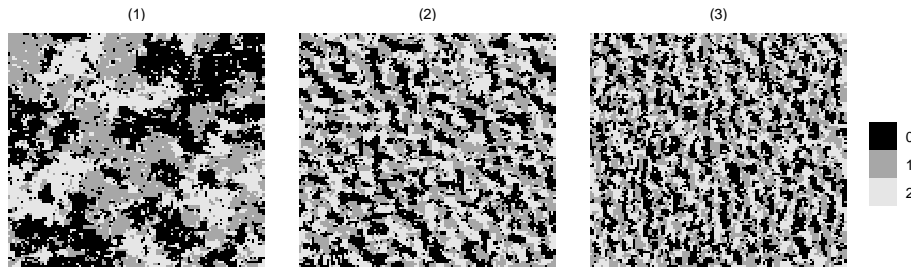


Figure 6: Simulated  $150 \times 150$  MRFs  $\mathbf{z}^{(i)}$ ,  $i = 1, 2, 3$ .

Table 1:  $\theta_{a,b,\mathbf{r}}$  used in simulations.

$\mathbf{r}$	$a$	$b = 0$	$b = 1$	$b = 2$	$\mathbf{r}$	$a$	$b = 0$	$b = 1$	$b = 2$
(1, 0)	0		-1.0	-1.0	(1, 0)	0		-1.0	-1.0
	1	-1.0	0.0	-1.0		1	-1.0	0.0	-1.0
	2	-1.0	-1.0	0.0		2	-1.0	-1.0	0.0
(3, 3)	0		0.3	0.3	(2, 0)	0		0.3	0.3
	1	0.3	0.0	0.3		1	0.3	0.0	0.3
	2	0.3	0.3	0.0		2	0.3	0.3	0.0

**Prior Distributions and Algorithm tuning.** For the RPS prior distribution, we considered  $q(\mathcal{R})$  a uniform distribution with every possible RPS that is a subset of the maximal RPS having the same probability, which represents a non-informative prior and also simplifies the computation of acceptance probabilities. Since the coefficients themselves are hardly interpretable, we chose to use vague priors for the varying-dimensional vector  $\theta$ , considering independent Gaussian priors with mean 0 variance and prior variance of  $\sigma_p^2 = 100$  for each of its components, regardless of the RPS associated with it.

As for the parameters involved in the proposal kernel, we executed multiple short pilot runs to evaluate whether high pseudoposterior regions (RPS and coefficients) were reached within a reasonable number of iterations. We concluded that  $\sigma_s = \sigma_{\text{bd}} = 0.15$ ,  $\sigma_w = 0.005$  and  $\nu = 0.1$  resulted in good balance between exploring the complex space that is composed by the RPS and the varying-dimension coefficient vector while maintaining the acceptance rate at reasonable levels.

For the mixture probabilities probabilities, we chose  $p_\Psi(\mathcal{R})$  always proportional to 4 for  $\Psi = w$  and 1 for the remaining types of moves that are valid for the current state  $\mathcal{R}$ , resulting in

$$\begin{aligned}
 p_w(\mathcal{R}) &\propto 4\mathbb{1}(\mathcal{R} \neq \emptyset), & p_{\text{bd}}(\mathcal{R}) &\propto 1, \\
 p_{\text{sw}}(\mathcal{R}) &\propto \mathbb{1}(\mathcal{R} \neq \mathcal{R}_{\text{max}}, \mathcal{R} \neq \emptyset), & & \\
 p_m(\mathcal{R}) &\propto \mathbb{1}(\mathcal{R} \neq \mathcal{R}_{\text{max}}, \mathcal{R} \neq \emptyset), \text{ and} & p_s(\mathcal{R}) &\propto \mathbb{1}(\mathcal{R} \neq \mathcal{R}_{\text{max}}, \mathcal{R} \neq \emptyset).
 \end{aligned} \tag{13}$$

It is important to note that not every type of move is defined for every RPS. For example, a random walk move cannot propose anything meaningful when  $\mathcal{R} = \emptyset$  and a swap move cannot be completed with  $\mathcal{R} = \mathcal{R}_{\text{max}}$ . This “prohibitions” introduced by setting some probabilities to zero ensure that we never propose moves that are not well defined and would not be able to change the state of the chain regardless.

We also explore the effect of the **initial state** of the chain by generating three independent chains for each simulation. In run 1, we start with all relative positions included and execute 5,000 warm-up iterations where only the random walk move, that does not change the RPS, is allowed. In run 2, we start with a nearest-neighbor RPS, and also run 5,000 warm-up iterations using only the random walk move. Finally, in run 3 we start with the empty RPS and run no

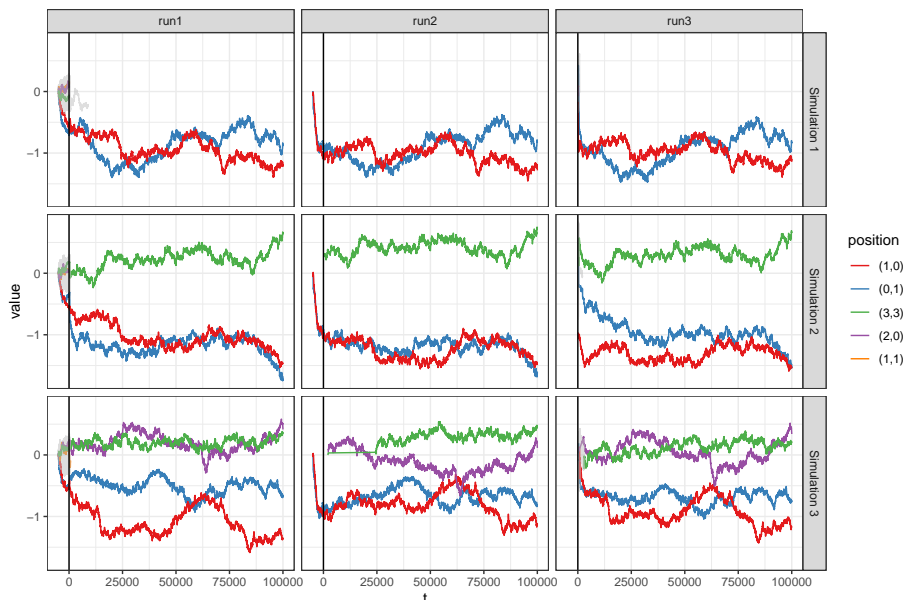


Figure 7: Values of the RJMCMC sampled for the interaction coefficients  $\theta_{\mathbf{r},1,0}$  for multiple relative positions  $\mathbf{r}$  in each simulation. Coefficients associated with set of relative positions are highlighted and colored and the remaining ones are represented with gray lines. Iterations of the warm-up run are indexed -4999 to 0.

warm-up iterations. Then, for all three runs, we perform 100,000 steps of the proposed Reversible-Jump MCMC algorithm.

**Results.** In all 9 simulations (3 initial states  $\times$  3 samples), the Markov chain sampled quickly reached the true RPS used in each one of the simulations, and the parameter values were also within a close range from the values in Table 1.

Figure 7 illustrates the sampled chain behavior in each simulation. Coefficients associated with some relevant positions are highlighted and colored so they can be tracked across iterations. The values for iterations in the warm-up stage (indexed by  $t < 0$ ) cannot be clearly identified as the coefficients for up to all 60 positions are included in this stage, but as the main Reversible Jump run starts, the number of positions included quickly reduces to no more than 4 within a few iterations. In this figure, lines may “appear” or “disappear” as relative positions are included or excluded, respectively, from the sampled RPS, and lines may change colors when swap moves are accepted.

These findings lead us to conclude that the Markov Chains generated by the RJMCMC algorithm quickly converged to the same RPS used to generate the data. Once this RPS was reached, this was the only RPS visited by the chain. This behavior is most likely due to the drastic reduction on the pseudoposterior

caused by the removal of any of the relative positions. On the other hand, the high-variance prior distributions for the additional coefficients included with a new position acts as a type of penalty that preventing positions from being included unless this inclusion increases the the pseudolikelihood significantly.

## 5 Application to Synthesis of Texture Image

To assess the effectiveness of the proposed model selection methodology within a practical data setting, we implement the algorithm on a discrete texture image obtained from the analysis of textile images in [Freguglia et al. \(2020\)](#). In the original work, a Gaussian mixture with 5 components, driven by the Markov Random Field model described in [Section 2](#), is used to describe grayscale continuous-valued images of dyed textiles and one of the products of the analysis is a pixel-wise segmentation of which mixture component was estimated as the most probable. The interaction coefficients of the hidden MRF were originally estimated considering a complete region, with every position within a maximum distance of 5, but we are interested in investigating whether similar interactions for the mixtures components could be described by a sparse interaction structure, producing synthetic texture images that have the same patterns as the reference image. We will consider the 200 by 200 subset of one of the estimated discrete images presented in [Figure 8](#), and denote it as  $\mathbf{z}^*$ .

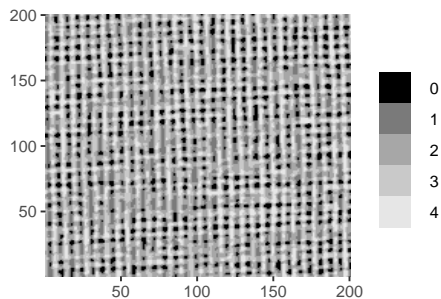


Figure 8: A 200 by 200 pixels texture image with 5 colors ( $C = 4$ ), denoted  $\mathbf{z}^*$ .

Considering the image data from [Figure 8](#), our goal is to determine whether the complete interaction structure is essential to properly describe the interactions of the observed random field, or if a sparse interaction structure could be used, without significant differences in terms of statistical inference. The search for sparse neighborhoods for modeling interactions in texture images has been the subject of several works in the literature, among them, [Cross and Jain \(1983\)](#) and [Gimel'farb \(1996\)](#). However, the selection methods employed in these studies are mostly heuristic.

To run the algorithm, we consider the maximal interaction structure of the algorithm,  $\mathcal{R}_{\max}$ , as the neighborhood used in the original paper, which includes positions with maximum norm up to 5. Hyper-parameters of prior distributions

and tuning parameters of the Reversible Jump algorithm were selected, based on several trial runs and the results observed in the simulations of [Section 4](#), to be  $\sigma_p = 1.5$ ,  $\sigma_s = \sigma_{bd} = 0.15$ ,  $\sigma_w = 0.005$  and  $\nu = 0.1$ .

Compared to the simulation study, the only parameter modified in this case is the variance of the prior distribution of the components of  $\theta$ , represented by  $\sigma_p^2$ . In practical terms, our goal is to keep all the positions which interaction is required to probabilistically describe the texture pattern, while at the same time controlling the number of free coefficients. This is achieved by selecting a RPS that is sparse when compared to the complete region originally used but explains the variability presented by the figure. The variance of such prior distributions ends up acting as a penalty on the value of the pseudoposterior for including new positions, even when their values are all close to 0, due to the new dimensions added to the probability measure being evaluated.

We ran 500,000 iterations of the proposed Reversible-Jump algorithm after 10,000 warm-up iterations. During the warm-up phase, the random walk move was selected with probability 1, starting from the maximal RPS. In the same way as described for the simulation study described in [Section 4](#), the warm-up iterations facilitated the initialization of the main RJMCMC run in a state close to the pseudoposterior mode for  $\mathcal{R}_{\max}$ .

The pseudoposterior probability sampled in the RJMCMC run for each relative position in  $\mathcal{R}_{\max}$  are presented in [Figure 9](#). Given the pseudoposterior distribution of the positions, we used the RPS threshold estimator strategy from [\(6\)](#) with a value of  $c_{\text{th}} = 0.4$  to select one sparse interaction structure to be used in our result analysis, with a reduction from 60 to 16 relative positions, which corresponds to a reduction of  $44 \times 24 = 1056$  free coefficients in the model. Other results could be drawn from RPS pseudoposterior distribution for model selection purposes, such as the set of highest pseudoposterior RPSs or the pseudoposterior probability of a group of RPSs with specific characteristics, depending on the type of analyses being made.

**Evaluating the results.** Unlike the analysis made for the simulation study presented in [Section 4](#), we do not know the interaction structure that generated the data, hindering direct comparison with the pseudoposterior distribution obtained with the RPS. Bayesian goodness of fit evaluation strategies as proposed in [Gelman et al. \(1996\)](#) and [Bayarri and Berger \(2000\)](#) involve generating realizations of the model by sampling from the posterior distribution and comparing key statistics from the reference dataset  $\mathbf{z}^*$  with those realizations using some prescribed metric. However, these methods are not directly applicable in our scenario as we only have access to the pseudoposterior distribution, rather than the true posterior distribution. Moreover, it is difficult to define a small number of key statistic to use for the tests, as MRF texture images have a high-dimensional vector of pairwise counts as sufficient statistics.

As an alternative approach to evaluate the sparse model obtained by thresholding the pseudoposterior distribution, we used maximum likelihood estimation via stochastic approximation, a standard inference method used in the context

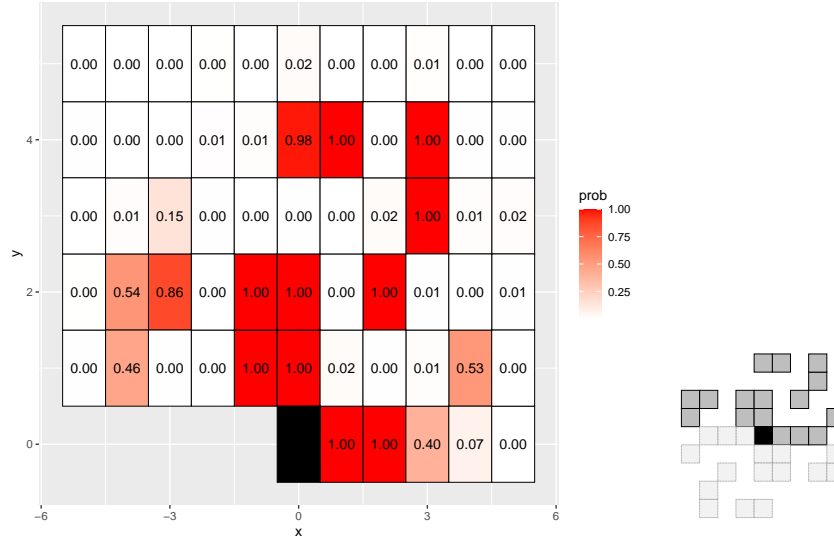


Figure 9: Map with the (rounded) proportions of times each relative position is included in the RPS sampled in the RJMCMC run (left) and the sparse interaction structure selected with a 0.4 threshold value  $\hat{\mathcal{R}}_{\text{sp}}(0.4)$  (right).

of MRFs. We then compared the results of such inference using the selected sparse interaction structure against the same analyses under other RPS. By applying maximum likelihood estimation under a predetermined RPS, we obtain the estimated coefficients. Subsequently, we generate realizations of the MRF using these estimated coefficients and compare useful statistics for describing the texture from the generated samples and the target dataset  $\mathbf{z}^*$ . This comparison provides insight into the effectiveness of the sparse interaction structure in capturing the underlying characteristics of the texture.

We considered 4 different reference RPSs for comparison:

1.  $\mathcal{R}_{\text{ind}} = \emptyset$ : The independent model, where each pixel is independent and has uniform distribution. In this case, there are no parameters to estimate.
2.  $\mathcal{R}_{\text{nn}} = \{(1, 0), (0, 1)\}$ : A nearest-neighbor RPS that we will use as a benchmark in comparisons.
3.  $\mathcal{R}_{\text{sp}}$ : The sparse RPS obtained using the thresholding estimator for our specific thresholding constant choice presented in [Figure 9](#).
4.  $\mathcal{R}_{\text{max}}$ : The maximal set of relative positions, containing all relative positions within maximum distance of 5, as used in the original paper.

and our goal is to evaluate whether completing an analysis using  $\mathcal{R}_{\text{sp}}$  leads to results at least as accurate as obtained using  $\mathcal{R}_{\text{max}}$ , and at the same time

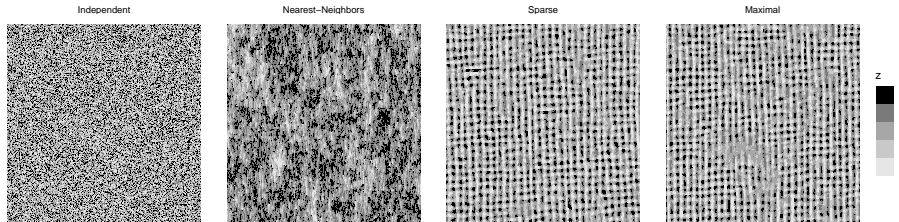


Figure 10: Simulated realizations of the MRF model under the independent case and using the estimates obtained by the Maximum Likelihood considering a Nearest-Neighborhood structure, Estimated Sparse interaction structure and Maximal interaction structure.

understand how relevant the differences were when compared to the estimates obtained when using a naive model choice with  $\mathcal{R}_{\text{nn}}$ .

We used the Stochastic Approximation algorithm (Robbins and Monro, 1951) to obtain a Maximum Likelihood estimate of the coefficients for each of the four described RPSs. The algorithm consists of iteratively updating the solution according to a step size sequence  $\gamma_{t \geq 0}^t$  and an estimate of the gradient function, that depends on the sufficient statistic of the model,  $T(\cdot)$ , computed on the reference dataset  $\mathbf{z}^*$  and on a realization,  $\mathbf{z}^{(t)}$ , of the random field simulated from the current coefficients (see Freguglia and Garcia (2022) for more details on the Stochastic Approximation algorithm used). The algorithm is described by the recursion

$$\boldsymbol{\theta}^{(t+1)} = \boldsymbol{\theta}^{(t)} + \gamma^{(t)} \left( T(\mathbf{z}^*) - T(\mathbf{z}^{(t)}) \right), \quad (14)$$

with  $\gamma^{(t)}$  being a decreasing sequence. Note that the sufficient statistics  $T(\cdot)$  has the same dimension as the vector of free coefficients  $\boldsymbol{\theta}$  and, therefore, its indexing also depends on the associated RPS. We used the proper definitions of  $T(\cdot)$  for each of the three RPSs used.

We ran 1500 steps of (14) with  $\gamma^{(t)} = \frac{1500-t}{1500}$  starting from the zero-valued coefficient vector  $\boldsymbol{\theta}_{a,b,\mathbf{r}} = 0$  for every  $a, b, \mathbf{r}$  for each of the three RPSs to obtain maximum likelihood estimates of coefficients in each case. Then, we generated 100 samples under each of three models with their respective estimated coefficients, which we will denote  $\tilde{\mathbf{z}}_{\text{ind}} = \left( \mathbf{z}_{\text{ind}}^{(v)} \right)$ ,  $\tilde{\mathbf{z}}_{\text{nn}} = \left( \mathbf{z}_{\text{nn}}^{(v)} \right)$ ,  $\tilde{\mathbf{z}}_{\text{sp}} = \left( \mathbf{z}_{\text{sp}}^{(v)} \right)$  and  $\tilde{\mathbf{z}}_{\text{max}} = \left( \mathbf{z}_{\text{max}}^{(v)} \right)$ ,  $v = 1, \dots, 100$ , for  $\mathcal{R}_{\text{ind}}$ ,  $\mathcal{R}_{\text{nn}}$ ,  $\mathcal{R}_{\text{sp}}$  and  $\mathcal{R}_{\text{max}}$  respectively, (the tilde symbol is used to stress the fact that it is a set of multiple MRF realizations). Examples of one of the simulated images for each of the three scenarios considered are presented in Figure 10. Notice that the first two image generated from the Independent and Nearest-Neighbor models completely miss the features of the texture, whereas there is not much difference between the one generated with the sparse model and the full one.

Finally, we define  $\rho_{a,b,\mathbf{r}}(\mathbf{z}) = \sum_{\mathbf{i} \in \mathcal{S}} \mathbb{1}(z_{\mathbf{i}} = a, z_{\mathbf{i}+\mathbf{r}} = b)$  as the count of

occurrences of the pair  $(a, b)$  within relative position  $\mathbf{r}$  (this is part of the vector of sufficient statistics of the model when  $\mathbf{r}$  is included in the RPS). To summarize this information, we compute the average counts for a set of realizations as

$$\bar{\rho}_{a,b,\mathbf{r}}(\tilde{\mathbf{z}}) = \sum_{v=1}^{100} \frac{\rho_{a,b,\mathbf{r}}(\mathbf{z}^{(v)})}{100},$$

and the metric

$$\Delta(\tilde{\mathbf{z}}, \mathbf{z}^*) = \log \left( \sqrt{\sum_{a \in \mathcal{Z}} \sum_{b \in \mathcal{Z}} \sum_{\mathbf{r} \in \mathcal{R}_{\max}} (\rho_{a,b,\mathbf{r}}(\mathbf{z}^*) - \bar{\rho}_{a,b,\mathbf{r}}(\tilde{\mathbf{z}}))^2} \right),$$

which represents the logarithm of the Euclidean distance between the vector containing all the pairwise counts for relative positions in the maximal RPS and the average vector of pairwise counts in the set of samples  $\tilde{\mathbf{z}}$  for the same relative positions. This is a measure of similarity between the patterns generated from each model and the observed sample  $\mathbf{z}^*$ . The smaller the value of  $\Delta(\tilde{\mathbf{z}}, \mathbf{z}^*)$ , the closest the pairwise counts of the reference field  $\mathbf{z}^*$  to their expected values (approximated by the samples average), under a model with that specific RPS and its associated maximum likelihood estimators for the coefficients. Note that we have used the counts in every relative position of the maximal RPS,  $\mathcal{R}_{\max}$ . This procedure ensures not only that the counts of relative positions included in the RPS used for estimation are similar to  $\mathbf{z}^*$ , but also provides a comparison across a larger common set of statistics across all three scenarios.

Table 2:  $\Delta(\tilde{\mathbf{z}}, \mathbf{z}^*)$  values considering the three sets of samples generated from the model estimated with different RPSs.

RPS	$\mathcal{R}_{\text{ind}}$	$\mathcal{R}_{\text{nn}}$	$\mathcal{R}_{\text{sp}}$	$\mathcal{R}_{\text{max}}$
$\Delta(\tilde{\mathbf{z}}, \mathbf{z}^*)$	10.643	10.989	8.641	8.969

As pointed before, looking at the generated samples displayed in [Figure 10](#), it is evident that the image generated from  $\mathcal{R}_{\text{nn}}$  has a pattern completely different from the original dataset  $\mathbf{z}^*$ , whereas both the examples generated  $\mathcal{R}_{\text{sp}}$  and  $\mathcal{R}_{\text{max}}$  display patterns very similar to  $\mathbf{z}^*$ . These visual observations are reflected in the computed values for  $\Delta(\tilde{\mathbf{z}}, \mathbf{z}^*)$  presented in [Table 2](#). As anticipated, the model estimated using the benchmark independent and nearest-neighbor structures resulted in the highest distance between pairwise counts of  $\mathbf{z}^*$  and their expected values in the model. On the other hand, the model estimated from  $\mathcal{R}_{\text{sp}}$  has their expected statistics closer to the observed in  $\mathbf{z}^*$  compared to the ones computed using  $\mathcal{R}_{\text{max}}$ .

Therefore, we conclude that estimating coefficients from a sparse interaction structure, obtained by thresholding the marginal RPS pseudoposterior distribution obtained from our proposed RJMCMC algorithm, yields superior results. This conclusion is true in terms of computational costs, since there was significantly less coefficients to compute, and in terms of how similar the expected

value of wide set of statistics is from the observed field used for estimation. The model estimated using the sparse structure produces images more similar to the reference than those generated by the model estimated using the complete structure, as it is shown by the reduced distance between the vectors of pairwise occurrences.

## 6 Conclusion

We propose a novel approach for model selection in Markov Random Field models with pairwise interactions within a Bayesian framework. Our method uses a Reversible Jump Markov Chain algorithm tailored with a proposal distribution specifically constructed to facilitate efficient jumping between sets of relative positions. This design quickly reaches the models with highest posterior mass.

In order to overcome the intractability of the normalizing constant inherent to MRF models, we use pseudolikelihood and proceed with the analyses based on the pseudoposterior distribution as a proxy for the true posterior distribution that cannot be directly evaluated. It is important to notice that the proposed algorithm can be directly adapted to accomodate different strategies that may be used to deal with the intractable constants and approximate likelihood functions, such as Adjusted Pseudolikelihoods (Bouranis et al., 2018a) and Monte-Carlo approximations (Atchadé et al., 2013). The key point is that the proposal kernel is designed for efficiency in this specific type of MRF distribution. It is worth noticing that not every approximation method is well suited for the varying-dimension feature inherent of the model selection framework.

The main contributions of this work are:

1. Proposing a Bayesian framework for the simultaneous estimation of the interaction structure and the parameters for the Markov Random Field model considered.
2. Constructing a Reversible Jump proposal kernel specifically tailored to accomodate the models within the proposed framework.
3. Demonstrating, through simulations and applications, the effectiveness of some choices of prior distribution and tuning parameters, while working under a flexible framework where different choices could be used with no additional changes to the algorithm.

We have used artificially generated datasets and an application to real data in the context of texture synthesis, to evaluate the strengths of our method and study how the algorithm behaves under different configurations. Our findings indicate promising results for selecting sparse interaction structures for MRFs.

For future directions, new methods for approximating the likelihood function (and the posterior distribution as a consequence) that can produce good approximations across the varying-dimension spaces, as an alternative to the pseudolikelihood would be an improvement on the proposed method. Additionally, conducting more detailed studies about the effects of the variance of

the prior distribution of  $\theta$  on the resulting RPS distribution could improve its performance.

The reproducible R language code used to generate all the results in this work is available upon request.

It leverages the data structures provided by the `mrf2d` package (Freguglia and Garcia, 2022).

## Acknowledgments

This work was funded by Fundação de Amparo à Pesquisa do Estado de São Paulo - FAPESP grants 2017/25469-2, 2017/10555-0, CNPq grant 304148/2020-2, and by Coordenação de Aperfeiçoamento de Pessoal de Nível Superior - Brasil (CAPES) - Finance Code 001.

## References

- Arnesen, P. and Tjelmeland, H. (2017). Prior specification of neighbourhood and interaction structure in binary markov random fields. *Statistics and Computing*, 27(3):737–756.
- Atchadé, Y. F., Lartillot, N., and Robert, C. (2013). Bayesian computation for statistical models with intractable normalizing constants. *Brazilian Journal of Probability and Statistics*, 27(4):416–436.
- Bayarri, M. and Berger, J. O. (2000). P values for composite null models. *Journal of the American Statistical Association*, 95(452):1127–1142.
- Besag, J. (1975). Statistical analysis of non-lattice data. *Journal of the Royal Statistical Society: Series D (The Statistician)*, 24(3):179–195.
- Blake, A., Kohli, P., and Rother, C. (2011). *Markov random fields for vision and image processing*. MIT press.
- Boland, A., Friel, N., and Maire, F. (2018). Efficient mcmc for gibbs random fields using pre-computation. *Electronic Journal of Statistics*, 12(2):4138–4179.
- Bouranis, L., Friel, N., and Maire, F. (2017). Efficient bayesian inference for exponential random graph models by correcting the pseudo-posterior distribution. *Social Networks*, 50:98–108.
- Bouranis, L., Friel, N., and Maire, F. (2018a). Bayesian model selection for exponential random graph models via adjusted pseudolikelihoods. *Journal of Computational and Graphical Statistics*, 27(3):516–528.
- Bouranis, L., Friel, N., and Maire, F. (2018b). Model comparison for gibbs random fields using noisy reversible jump markov chain monte carlo. *Computational Statistics & Data Analysis*, 128:221–241.

- Brooks, S. P., Giudici, P., and Roberts, G. O. (2003). Efficient construction of reversible jump markov chain monte carlo proposal distributions. *Journal of the Royal Statistical Society: Series B (Statistical Methodology)*, 65(1):3–39.
- Caimo, A. and Mira, A. (2015). Efficient computational strategies for doubly intractable problems with applications to bayesian social networks. *Statistics and Computing*, 25(1):113–125.
- Cross, G. R. and Jain, A. K. (1983). Markov random field texture models. *IEEE Transactions on Pattern Analysis and Machine Intelligence*, (1):25–39.
- Csiszár, I. and Talata, Z. (2006). Consistent estimation of the basic neighborhood of markov random fields. *The Annals of Statistics*, 34(1):123–145.
- Freguglia, V. and Garcia, N. L. (2022). Inference tools for Markov random fields on lattices: The R package mrf2d. *Journal of Statistical Software*, 101(8):1–36.
- Freguglia, V., Garcia, N. L., and Bicas, J. L. (2020). Hidden markov random field models applied to color homogeneity evaluation in dyed textile images. *Environmetrics*, 31(4):e2613.
- Gelman, A. and Meng, X.-L. (1998). Simulating normalizing constants: From importance sampling to bridge sampling to path sampling. *Statistical science*, pages 163–185.
- Gelman, A., Meng, X.-L., and Stern, H. (1996). Posterior predictive assessment of model fitness via realized discrepancies. *Statistica sinica*, pages 733–760.
- Geyer, C. J. and Thompson, E. A. (1992). Constrained monte carlo maximum likelihood for dependent data. *Journal of the Royal Statistical Society: Series B (Methodological)*, 54(3):657–683.
- Gimel'farb, G. L. (1996). Texture modeling by multiple pairwise pixel interactions. *IEEE Transactions on pattern analysis and machine intelligence*, 18(11):1110–1114.
- Green, P. J. (1995). Reversible jump markov chain monte carlo computation and bayesian model determination. *Biometrika*, 82(4):711–732.
- Green, P. J. and Richardson, S. (2002). Hidden markov models and disease mapping. *Journal of the American statistical association*, 97(460):1055–1070.
- Gu, M. G. and Zhu, H.-T. (2001). Maximum likelihood estimation for spatial models by markov chain monte carlo stochastic approximation. *Journal of the Royal Statistical Society Series B: Statistical Methodology*, 63(2):339–355.
- Hassner, M. and Sklansky, J. (1981). The use of markov random fields as models of texture. In *Image Modeling*, pages 185–198. Elsevier.

- Held, K., Kops, E. R., Krause, B. J., Wells, W. M., Kikinis, R., and Muller-Gartner, H.-W. (1997). Markov random field segmentation of brain mr images. *IEEE transactions on medical imaging*, 16(6):878–886.
- Ji, C. and Seymour, L. (1996). A consistent model selection procedure for markov random fields based on penalized pseudolikelihood. *The annals of applied probability*, 6(2):423–443.
- Kato, Z., Zerubia, J., et al. (2012). Markov random fields in image segmentation. *Foundations and Trends® in Signal Processing*, 5(1–2):1–155.
- Lee, J. D. and Hastie, T. J. (2013). Structure learning of mixed graphical models. *Journal of Machine Learning Research*, 31:388–396.
- Liang, F. (2007). Continuous contour monte carlo for marginal density estimation with an application to a spatial statistical model. *Journal of Computational and Graphical Statistics*, 16(3):608–632.
- Murray, I., Ghahramani, Z., and MacKay, D. (2012). Mcmc for doubly-intractable distributions. *arXiv preprint arXiv:1206.6848*.
- Pensar, J., Nyman, H., Niiranen, J., and Corander, J. (2017). Marginal pseudo-likelihood learning of discrete markov network structures. *Bayesian analysis*, 12(4):1195–1215.
- Robbins, H. and Monro, S. (1951). A stochastic approximation method. *The annals of mathematical statistics*, pages 400–407.
- Roy, A. and Dunson, D. B. (2020). Nonparametric graphical model for counts. *Journal of Machine Learning Research*, 21(229):1–21.
- Su, C. and Borsuk, M. E. (2016). Improving structure mcmc for bayesian networks through markov blanket resampling. *The Journal of Machine Learning Research*, 17(1):4042–4061.
- Zhang, Y., Brady, M., and Smith, S. (2001). Segmentation of brain MR images through a hidden markov random field model and the expectation-maximization algorithm. *IEEE transactions on medical imaging*, 20(1):45–57.
- Zhu, W. and Fan, Y. (2018). A novel approach for markov random field with intractable normalizing constant on large lattices. *Journal of Computational and Graphical Statistics*, 27(1):59–70.